Ecotoxicology and Environmental Safety 267 (2023) 115633

Contents lists available at ScienceDirect

Ecotoxicology and Environmental Safety

journal homepage: www.elsevier.com/locate/ecoenv

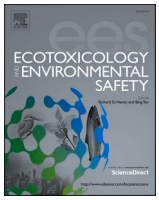

Nitro-oxidative response to internalized multi-walled carbon nanotubes in *Brassica napus* and *Solanum lycopersicum*

Zsuzsanna Kolbert [a,*,1], Árpád Molnár [a,1], Kamilla Kovács [a], Sára Lipták-Lukácsik [a], Péter Benkő [b,c], Réka Szőllősi [a], Katalin Gémes [a,c], László Erdei [a], Andrea Rónavári [d], Zoltán Kónya [d]

[a] Department of Plant Biology, University of Szeged, Közép fasor 52., 6726, Szeged, Hungary
[b] Doctoral School of Biology, Faculty of Science and Informatics, University of Szeged, Közép fasor 52., 6726, Szeged, Hungary
[c] Institute of Plant Biology, Biological Research Centre, HUN-REN, Temesvári körút 62., 6726, Szeged, Hungary
[d] Department of Applied and Environmental Chemistry, Faculty of Science and Informatics, University of Szeged, Rerrich Bela ter 1., 6720 Szeged, Hungary

ARTICLE INFO

Edited by R Pereira

Keywords:
Brassica napus
Solanum lycopersicum
Nitro-oxidative stress
Multi-walled carbon nanotubes

ABSTRACT

In addition to their beneficial effects on plant physiology, multi-walled carbon nanotubes (MWCNTs) are harmful to plants in elevated concentrations. This study compared the effects of two doses of MWCNT (10 and 80 mg/L) in *Brassica napus* and *Solanum lycopersicum* seedlings focusing on nitro-oxidative processes. The presence of MWCNTs was detectable in the root and hypocotyl of both species. Additionally, transmission electron microscopy analysis revealed that MWCNTs are heavily transformed within the root cells forming large aggregates. The uptake of MWCNTs negatively affected root viability and root cell proliferation of both species, but more intense toxicity was observed in *S. lycopersicum* compared to *B. napus*. The presence of MWCNT triggered more intense protein carbonylation in the relative sensitive *S. lycopersicum*, where increased hydrogen peroxide levels were observed. Moreover, MWCNT exposure increased the level of physiological protein tyrosine nitration which was more intense in *S. lycopersicum* where notable peroxynitrite accumulation occurred. These suggest for the first time that MWCNT triggers secondary nitro-oxidative stress which contributes to its toxicity. Moreover, the results indicate that the extent of the nitro-oxidative processes is associated with the extent of MWCNT toxicity.

1. Introduction

Carbon nanotubes (CNTs) are carbon-based, tube-like nanomaterials in which graphene forms bundles of single (single-walled carbon nanotubes) or multiple sheets (multi-walled carbon nanotubes, MWCNTs). The diameter of MWCNTs ranges from a 5–100 nm (He et al., 2013) and the length of several hundred nanometers to several micrometers. Due to their unique structural, optical, electronic and mechanical features, CNTs including MWCNTs are one of the most studied engineered nanomaterials (NMs). CNTs are widely utilized in biomedicine, nanoelectronics, bioengineering, mechanical engineering and their application possibilities have been expanded to health care and agriculture. Regarding the phytoeffects of CNTs, the interaction of the NMs with plant cells is of great significance. It has been reported in multiple plant species, that the cell wall is penetrable to CNTs meaning that CNTs including MWCNTs can be internalized by plant cells (Lin et al., 2009; Liu et al., 2009; Khodakovskaya et al., 2013; Lahiani et al., 2013; Martínez-Ballesta et al., 2016; Hu et al., 2021; Yang et al., 2021).

During plant cultivation, MWCNT treatment has a good potential for inducing seed germination and increasing vegetative and reproductive growth. In several crop species, MWCNTs increase germination rate, root and shoot growth, leaf number, flower and fruit production (reviewed by Mathew et al., 2021). As for the molecular mechanisms of germination/growth induction, MWCNTs increase water uptake due to the intensified expressions of aquaporin genes (*e.g. PIP1* and *PIP2*, Cherati et al., 2021), enhance the expression of genes involved in cell division and cell wall extension, intensify sugar metabolism and antioxidant defence, and induce lipid remodelling (reviewed by Szőllősi et al., 2020). Recently, MWCNTs have been found to regulate the key enzymes involved in carbon (*e.g.* phosphoenolpyruvate carboxylase)

* Corresponding author.
E-mail address: ordogne.kolbert.zsuzsanna@szte.hu (Z. Kolbert).
[1] These authors contributed equally to this work

https://doi.org/10.1016/j.ecoenv.2023.115633
Received 15 March 2023; Received in revised form 14 October 2023; Accepted 22 October 2023
Available online 25 October 2023
0147-6513/© 2023 The Authors. Published by Elsevier Inc. This is an open access article under the CC BY-NC-ND license (http://creativecommons.org/licenses/by-nc-nd/4.0/).

and nitrogen (*e.g.* nitrate reductase) metabolism thus promoting the carbohydrate production and nitrogen utilization resulting in improved plant growth (Hu et al., 2021). Beyond growth promotion, MWCNT exposure may result also in phytotoxicity due to direct interaction of genomic DNA (Khalifa, 2018) or decreased auxin, gibberellin, cytokinin, jasmonic acid, abscisic acid and brassinolide levels (Hao et al., 2016). Moreover, MWCNTs induce oxidative stress processes like the over-production of reactive oxygen species (ROS, *e.g.* hydrogen peroxide, H_2O_2), the activation of antioxidant defense (*e.g.* superoxide dismutase, ascorbate peroxidase *etc.*) and the peroxidation of membrane lipids (*e.g.* Lin et al., 2010; Rahmani et al., 2020: Li et al., 2022). Besides lipids, proteins are also affected by oxidative modifications. Protein carbonylation a non-enzymatic and irreversible post-translational modification (PTM) is a key process in oxidative signalling, which affects plant proteome under stress (Tola et al., 2021). Results suggest that H_2O_2 accumulation is responsible for changes in physiological protein carbonylation (Fangue-Yapseu et al., 2022). Reactive oxygen species-related oxidative processes are in close connection with reactive nitrogen species (RNS) such as nitric oxide (NO), peroxynitrite ($ONOO^-$) or *S*-nitrosoglutathione (GSNO). The GSNO plays a major role in NO signalling and its concentration is partly regulated by GSNO reductase enzyme (GSNOR, Jahnová et al., 2019). GSNOR has also been proposed as a regulator of oxidative stress due to its capability for oxidative PTM (Li et al., 2021). During stress, RNS overproduction can modify a large variety of biologically relevant macromolecules (proteins, nucleotides and fatty acids) resulting in secondary nitrosative stress (Valderrama et al., 2007). The most prevalent nitrosative modification is protein tyrosine nitration, which can inhibit protein function and is a significant factor during abiotic stresses (Kolbert et al., 2017; Corpas et al., 2021).

The nitro-oxidative processes in plants in response to MWCNT treatment has not been uncovered yet. To evaluate the involvement of nitro-oxidative signalling in the plant responses to MWCNTs, we compared ROS and RNS levels, metabolism, protein carbonylation and tyrosine nitration in two agricultural plant species (*Brassica napus* and *Solanum lycopersicum)* with different sensitivity.

2. Materials and methods

2.1. Synthesis and characterization of MWCNTs

All chemicals were obtained from Sigma-Aldrich and used as received. The MWCNTs were prepared using the catalytic chemical vapor deposition (CCVD) procedure described previously (Smajda et al., 2007). Briefly, 2.5–2.5% of Co, Fe containing alumina supported catalyst was placed in a quartz boat into the reactor tube. The system was purged with pure nitrogen at 1000 K and then the gas stream was changed to acetylene–nitrogen (1:10) mixture. The flow rate of the acetylene was 15 cm^3/min and the reaction lasted for 1 h. After this, the system was cooled under nitrogen flow and the sample was purified by first adding cc. NaOH solution to dissolve the alumina support, then treated in cc. HCl solution to remove the metal particles, after that the oxidation step by adding 0.1 molar equivalent $KMnO_4$ to 0.1 M H_2SO_4 solution and lastly the sample was dried.

To assess the size and morphological characteristics of the nanotubes, transmission electronic microscopy (TEM) analyses were performed on a FEI Tecnai G^2 20 X-Twin instrument (FEI Corporate Headquarters, Hillsboro, OR, USA) at accelerating voltage of 200 kV. Samples for TEM investigations were prepared by drop-coating MWCNTs suspension on carbon-coated copper TEM grids. The crystal structure of MWCNTs was identified by X-ray diffraction (XRD) measurement in a Rigaku equipment with an acquisition in the radiation incidence angle range of 10–80°, the scanning rate was 2°min^{-1}.

2.2. Plant growing conditions and treatments

To analyse the effect of MWCNT treatment, two agronomically important plant species were used: oilseed rape (*Brassica napus* L. cv. GK Gabriella) and tomato (*Solanum lycopersicum* cv. Manó). Seeds were surface sterilised with 70% (v/v) ethanol for 1 min and with 5% (v/v) sodium hypochlorite for 10 min. To remove excess chemicals, seeds were washed four times with sterile distilled water and placed on filter paper in sterile Petri dishes. Treatment was administered through the filter paper; it was moistened either with distilled water (control) or MWCNT suspension. Due to the hydrophobic nature of MWCNTs, first we produced a 100 mg/L stock of MWCNTs in distilled water and dispersed it for 30 min with an ultrasound sonicator. After setting the concentration to the desired 10 mg/L or 80 mg/L, another 30 min sonication occurred. Treatment solution was immediately measured on filter papers, to ensure homogenous MWCNT concentration. *Brassica napus* was grown for 5 days, while *S. lycopersicum* was grown for 7 days before sample collection, in a greenhouse with controlled conditions (150 μmol/m^2/s or 150 μmol m^{-2} s^{-1} photon flux density with 12 h/12 h light/dark cycle, relative humidity 55–60% and temperature 25 ± 2 °C).

2.3. Studying MWCNTs in plant tissues

Two mm long segments for TEM analysis were collected from mature root sections, the lower and upper part of the hypocotyl. Samples were fixed in 3% glutaraldehyde prepared in PBS buffer (pH 7.4). Fixed plant material was embedded in Embed812 (EMS, USA) and cut to 70 nm thin sections with Ultracut S ultra-microtome (Leica, Austria). Sections were labelled with uranyl acetate and lead citrate and analysed with a Jeol 1400 plus transmission electron microscope (Jeol, Tokyo, Japan).

Raman spectra were recorded with a Bruker Sentera II confocal Raman microscope using a laser source with 785 nm excitation laser with a power of 1 mW. The spectral resolution was 4 cm^{-1}, 3 spectra, collected for 10 s each, were averaged.

2.4. Cell viability and proliferation analysis

To evaluate roots meristem cell viability fluorescein diacetate (FDA) fluorophore was used. Root tips (0.5 cm long) were labelled with 10 μM staining solution (prepared in 10/50 mM MES/KCl buffer, pH 6.15) for 30 min in the dark. After washing four times with MES buffer, samples were put on slides for visualisation. Viability of the meristem was expressed in percentage of the fluorescent intensity measured in control samples.

To label cell nuclei in S-phase, 5-ethynyl-2′-deoxyuridine (EdU) was used, similar to Nakayama et al. (2015). Root segments were incubated for 4 h in 20 μM EdU solution (prepared in PBS pH 7.4) at room temperature in darkness. EdU solution was changed to detergent buffer (PBS buffer containing 4% formaldehyde and 0.5% Triton X-100) for 30 min and samples were washed three times with PBS. Root tips were transferred for 2 h to the reaction mix, which contained 4 mM $CuSO_4$, 40 mM ascorbate and 3,62 μM Alexa fluor 488 azide. Samples were washed three times with PBS, put on slides for microscopic analysis.

2.5. Detection of ROS and RNS levels in roots by microscopy

The 10-acetyl-3,7- dihydroxypenoxazine Amplex Red (AR) fluorescent probe was used for the visualisation of H_2O_2. Root segments were stained in 50 μM AR solution (prepared in sodium phosphate buffer pH 7.5) at room temperature in the dark for 30 min and washed once before microscopic analysis (Kolbert et al., 2012).

4-amino-5-methylamino-2′,7′-difluorofluorescein diacetate (DAF-FM DA) was used to visualise NO levels. Samples were incubated in 10 μM DAF-FM DA solution (prepared in 10 mM Tris-HCl buffer, pH 7.4) for 30 min. After washing twice with the same buffer samples were put on slides (Kolbert et al., 2012).

The immunofluorescent detection of GSNO was performed on root segments collected from mature root zones. Plant tissues were fixated with 4% paraformaldehyde, embedded in 5% bacterial agar and cut to

100 μm thick cross-sections with a vibratome (VT 1000 S, Leica), and immunodetection was performed according to Corpas et al. (2008) with slight modifications. The sections were labelled overnight at room temperature with rat anti-GSNO primary antibody (1:2500 dilution in TBSA-BSAT buffer, pH 7.2, containing 5 mM Tris, 0.9% NaCl, 0.05% sodium azide, 0.1% BSA and 0.1% Triton X-100). After three washing steps with TBSA-BSAT, the secondary FITC conjugated antibody was administered for 1 h. For microscopic analysis, samples were transferred to slides in PBS:glycerine (1:1).

For peroxynitrite detection, root tips were labelled for 30 min within 10 μM aminophenyl fluorescein (APF) solution (prepared in 10 mM Tris-HCl buffer, pH 7.4). Before microscopic analysis samples were washed twice (Chaki et al., 2009 with slight modification).

Microscopic equipment consisted of a Zeiss Axiovert 200 M inverted microscope (Carl Zeiss, Jena, Germany) and a digital camera (Axiocam HR, HQ CCD, Carl Zeiss, Jena, Germany). Green fluorophores (FDA, Alexa fluor 488, DAF-FM DA, APF, FITC) were visualised with filter set 10 (exc.: 450–490, em.: 515–565 nm), and for detecting AR we used filter set 20HE (exc.: 546/12 nm, em.: 607/80 nm). We quantified pixel intensities in circles using Axiovision Rel. 4.8 software (Carl Zeiss, Jena, Germany).

2.6. Protein extraction, western blot analysis of protein abundance and modifications

Samples for proteomic analysis were ground with extraction buffer (50 mM Tris–HCl buffer, pH 7.6–7.8 with 0.1 mM EDTA, 0.1% Triton X-100% and 10% glycerol). After centrifugation (4 °C, 9300 × *g*, 20 min) the supernatant was treated with 1% plant protease inhibitor cocktail, and used for western blotting except protein carbonylation. Bradford (1976) assay was used to determine protein concentration.

Western blot analyses for protein abundance and tyrosine nitration were performed similarly. Denaturated protein samples (for ascorbate peroxidase [APX] 10 μg, for GSNOR detection 12.5 μg and for tyrosine nitration 15 μg) were separated on 12% SDS-PAGE gels, transferred to PVDF membrane using tank transfer technique (25 mA 16 h) and blocked with 5% non-fat milk. Primary antibody labelling has been done by the appropriate polyclonal rabbit antibody in dilution of 1:2000 (anti-APX: Agrisera, cat. No. AS 08 368, anti-GSNOR: Agrisera, cat. No. AS09 647, anti-3-nitrotyrosine: Sigma-Aldrich, cat. No. N0409). Secondary antibody labelling was performed with goat anti-rabbit IgG–alkaline phosphatase (1:10000 dilution) and membranes were developed with NBT/BCIP (5-bromo-4-chloro-3-indolyl phosphate) reaction. The method is described in detail in Kolbert et al. (2018).

Carbonyl groups were labelled with DNPH prior to western blotting using Abcam's oxidized protein assay kit (ab 178020). Samples were homogenized with 1x extraction buffer (containing 50 mM DTT) and incubated on ice for 20 min. After centrifugation (4 °C, 18000 × *g*, 20 min), the protein concentration of the supernatant was measured. 10 μL of sample was derivatized with 1x DNPH solution for 20 min and as a negative control 1x derivatization control solution were applied to aliquot. The reaction was stopped with neutralisation solution and 7.5 μg of proteins from both DNPH labelled and negative control samples were subjected to SDS-PAGE. Transfer to PVDF membranes was performed similarly to normal western blotting, membranes were labelled with the provided anti-DNP antibody for 1 h. The secondary antibody labelling and development has been performed similarly to the normal western blot. The method is described in detail in Molnár et al. (2020).

2.7. Cell wall peroxidase, APX and GSNOR activity analysis

Total apoplastic cell wall peroxidase activity was visualised with pyrogallol (Eleftheriou et al., 2015). Root samples were labelled for 15 min in staining solution (0.2% pyrogallol, 0.03% H_2O_2 dissolved in 10 mM phosphate buffer, pH 7.0) and washed twice with distilled water.

APX activity was measured similarly to the method of Nakano and Asada (1981). Plant samples were ground with 1:6 vol extraction buffer and centrifuged (4 °C, 9300 x g, 20 min). The method is based on that APX oxidizes ascorbate in the presence of H_2O_2, which can be detected at 265 nm. Enzyme activity is expressed as unit/g fresh weight.

GSNOR enzyme activity was measured by observing the NADH depletion in the reaction mixture at 340 nm (Sakamoto et al., 2002). GSNOR enzyme extract was acquired by homogenizing samples with 1:4 vol of buffer (0.1 M Tris-HCl, pH 7.5, containing 2 mM DTT, 0.1 mM EDTA, 0.2% Triton X-100% and 10% glycerine), centrifuged (4 °C, 9300 x g, 20 min). This extract was added to the reaction mixture (20 mM Tris–HCl, pH 8.0, 0.5 mM EDTA, 0.2 mM NADH and 0.4 mM GSNO). Data are expressed as nmol NADH min/mg/protein.

2.8. Analysis of gene expression by qRT-PCR

For RNA extraction, roots were frozen in liquid nitrogen and stored on − 80 °C. Samples were homogenized in liquid nitrogen for RNA extraction with Quick-RNA Miniprep Kit (Zymo Research, Irvine, CA, US), according to provided instructions. Isolated RNA-s quality and quantity were analysed with NanoDrop™2000/2000c spectrophotometer (Thermo Fisher Scientific, Waltham, MA, USA) and 1 μg was used for reverse-transcription with RevertAidFirst Strand cDNA Synthesis Kit (Thermo Fisher Scientific). Primer design was performed with NCBI primer design tool (Ye et al., 2012) and the acquired sequences are shown in Table S1. Quantitative reverse transcription (qRT)-PCR was performed using CFX384 Touch Real-Time PCR Detection System (Bio-Rad Laboratories Inc., Hercules, CA, USA) in Hard-Shell®384-well plates (thin-wall, skirted, white; Bio-Rad, Cat. no: HSP3805) and the reaction mixtures in each well had a final volume of 7 μL. For primary data analysis Bio-Rad CFX Maestro (Bio-Rad) software was used. The relative mRNA levels were calculated using the $2^{-\Delta\Delta Ct}$ method in Microsoft Office Excel 2016.

2.9. Statistical analysis

All shown results are mean values of raw data with (± SE or ± SD). Student's *t*-test or Duncan's multiple range test (OneWay ANOVA, $P < 0.05$) were used in SigmaPlot 12 for statistical evaluation of data. For the assumptions of ANOVA we used Hartley's F_{max} test for homogeneity and the Shapiro-Wilk normality test.

3. Results and discussion

3.1. Characterization of synthesized MWCNTs

The TEM images (Fig. 1A) demonstrate that the MWCNTs were over 10 μm in length with outer and inner diameters of 10–25 nm and 3–6 nm, respectively. The XRD profile obtained for MWCNTs (Fig. 1B) showed the typical reflections of the planes (002) and (100) at 2θ equal to 26.04° and 43.37°, respectively. The first peak indicates the presence of the effect of different overlapping graphene sheets, characteristic of multi-layered carbon nanotubes (JCPDS No. 01–0646, Abdel-Ghani et al., 2015) In addition, such peaks are broad, characteristic of amorphous materials, as expected for carbon nanotubes.

3.2. MWCNTs are internalized in seedlings of both species

In the cytoplasm and vacuoles of root cells of MWCNT-exposed *B. napus* and *S. lycopersicum*, the presence of elongated, electrondense structures was observed (indicated by red arrows in Fig. 2 B,C,D,F,G,H). These structures were not present in the untreated samples (Fig. 2A and E) suggesting that MWCNTs are internalized and created large, hydrophobic barriers most likely disrupting cell homeostasis. Moreover, in case of 80 mg/L MWCNT exposure, spherical structures were detected in the apoplast of *B. napus* root cells (indicated by a red arrow in Fig. 2C). We observed star-like structures most likely consisting of MWCNTs and

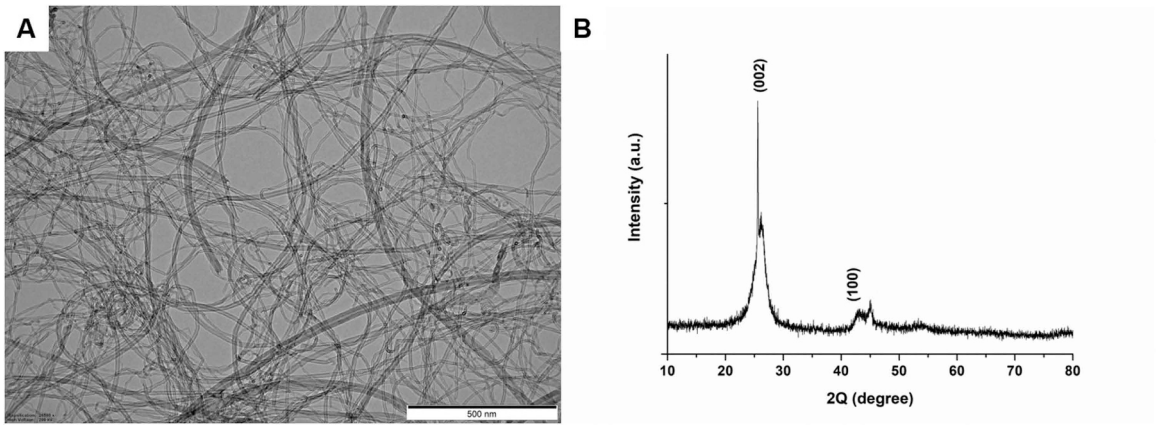

Fig. 1. Representative TEM image (A, scale= 500 nm), and X-ray diffractogram (XRD) of the MWCNTs (B).

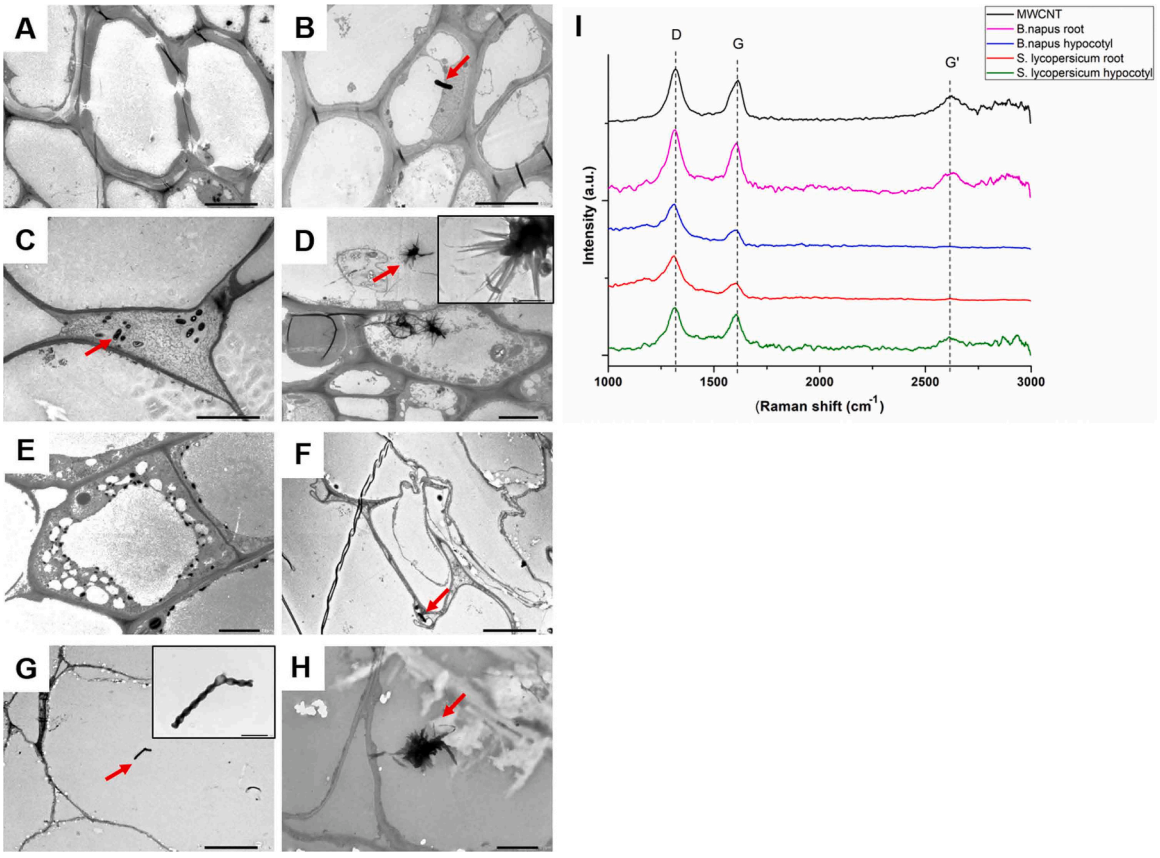

Fig. 2. TEM images of cells from *B. napus* (A-D) and *S. lycopersicum* (E-H). Root cells of control (A, scale=10 μm), 10 mg/L (B, scale=5 μm) or 80 mg/L (C, scale=5 μm) MWCNT-treated *B. napus*. Representative sample of *B. napus* upper hypocotyl showing star-shaped structures (D, scale=5 μm, inlet scale=500 nm). Root cells of control (E, scale=2 μm), 10 mg/L (F, scale=10 μm) or 80 mg/L (G, scale=10 μm, inlet scale= scale=1 μm) MWCNT-treated *S. lycopersicum*. Representative sample of *S. lycopersicum* upper hypocotyl showing a star-shaped structure (H, scale=2 μm). Electrondense structures correspondent to MWCNTs are indicated by red arrows. Raman spectroscopy analysis of MWCNT and 80 mg/L MWCNT-treated plant samples (I).

adhered macromolecules in cell vacuoles of the upper hypocotyl of both species (indicated by red arrows in Fig. 2D and H). This supports the possibility of MWCNT translocation to cotyledons and leaves (Larue et al., 2012; Chen et al., 2015). Similar to our observations, intracellular aggregates and plaques were detected in other plant systems exposed to MWCNTs (*e.g.* Smirnova et al., 2012; Gohari et al., 2020) indicating that the internalized MWCNTs may be heavily modified within the cells.

Due to the results of Raman analysis, the spectra of all samples showed the presence of the disorder or D-band (~1320 cm^{-1}) along with the characteristic graphitic band or G-band (~1610 cm^{-1}). These bands are characteristic to MWCNT and were detected both in the root and in the hypocotyl of *B. napus* and *S. lycopersicum* (Fig. 2I) supporting the internalization and translocation of MWCNTs to the aerial parts in both species. Our results support those of Larue et al. (2012) where root uptake and root-to-shoot translocation of MWCNTs in hydroponically-grown *Triticum aestivum* and *B. napus* were demonstrated using TEM and Raman analyses. Additionally, in accordance to our results several authors have demonstrated the uptake of MWCNTs in diverse plants systems (recently reviewed by Safdar et al., 2022).

3.3. The uptake of MWCNTs negatively affects key cellular processes

The internalized MWCNTs only slightly influenced plant growth parameters (seedling fresh and dry weights, root and hypocotyl lengths, data not shown) without exerting negative effects. This is most likely due to the early growth stage during which the seedlings use the stored nutrients of the seed. In contrast, endogenous cellular processes, such as root meristem cell viability and root cell proliferation changed considerably in response to the treatments. Root meristem cell viability decreased only slightly (by 28%) in case of 80 mg/L MWCNT-exposed *B. napus* seedlings (Fig. 3 AC). Additionally, *B. napus* retained ~60 and ~56% cell proliferation rate in the presence of 10 and 80 mg/L MWCNT, respectively (Fig. 3 BC). In *S. lycopersicum* roots, even in case of 10 mg/L MWCNT meristem cell viability decreased by 60% compared to control, while the higher MWCNT dosage caused 68% viability loss (Fig. 3 AC). The EdU-positive signal in the root tips of *S. lycopersicum* seedlings decreased drastically, especially with the 80 mg/L MWCNT treatment, where proliferation rate was reduced by about 75% (Fig. 3BC). This implies that both concentrations of MWCNTs exert toxic effects on cells which are more pronounced in *S. lycopersicum* compared to *B. napus*.

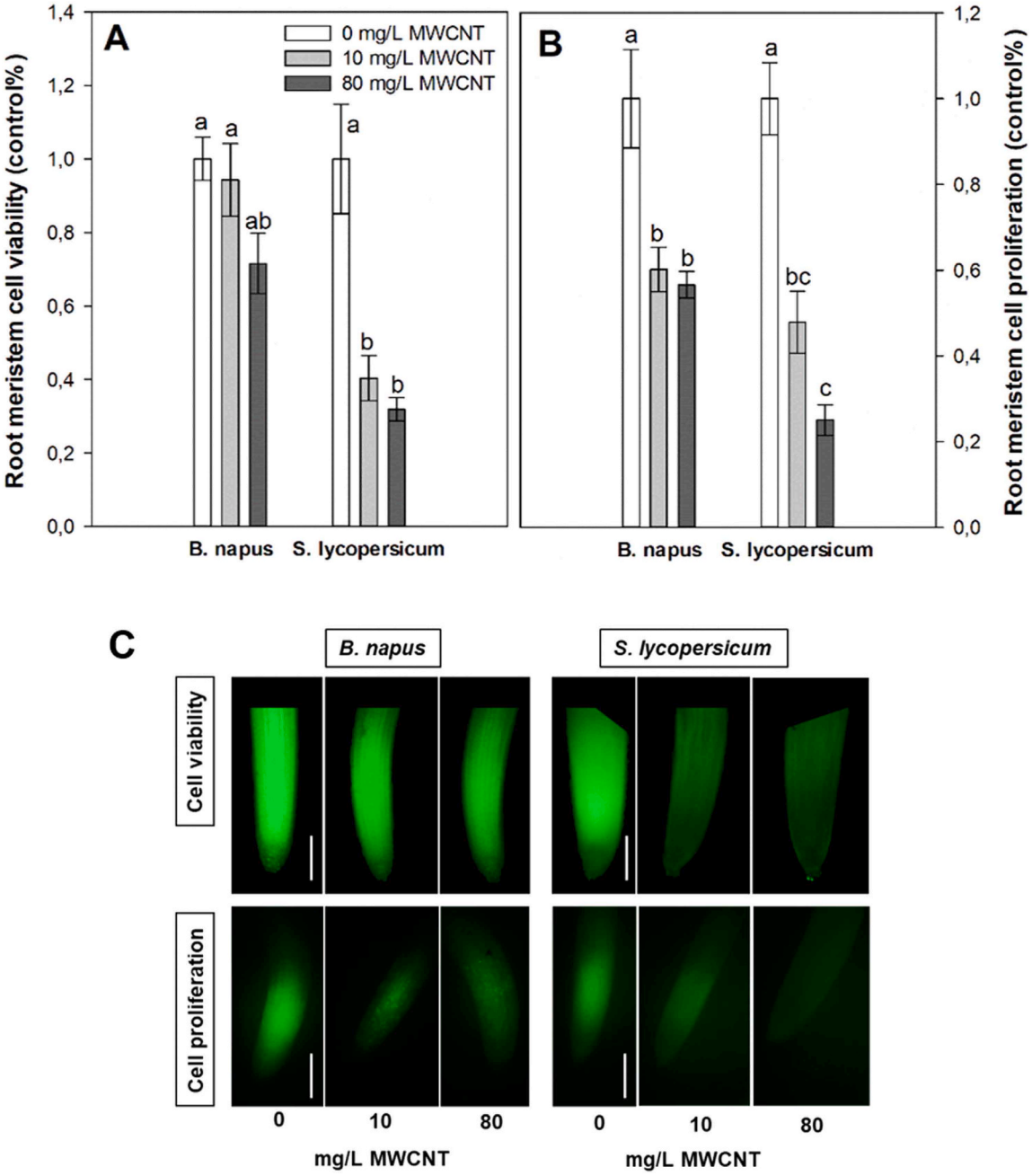

Fig. 3. (A) Viability of root meristem cells in *B. napus* and *S. lycopersicum* seedlings grown in the presence of 0 (control), 10 or 80 mg/L MWCNT for 5 days. Data are expressed in control %, and different letters indicate significant differences according to Duncan's test ($n = 10$, $P \leq 0.05$). (B) Cell proliferation rate visualized by EdU staining. Data are expressed in control %, and different letters indicate significant differences according to Duncan's test ($n = 10$, $P \leq 0.05$). (C) Representative microscopic images taken from the root tips of control and MWCNT-exposed *B. napus* and *S. lycopersicum* seedlings labelled with FDA (cell viability) or EdU (cell proliferation) fluorophores. Scale= 250 μm.

3.4. MWCNTs induce protein carbonylation accompanied by H_2O_2 accumulation despite of peroxidase activation

The toxicity of MWCNTs is associated with oxidative damage due to ROS accumulation. Interestingly, MWCNTs did not modify H_2O_2 levels in *B. napus* roots (Fig. 4A). In contrast, in *S. lycopersicum* H_2O_2 levels increased by ~70% and ~120% compared to control as the effect of 10 and 80 mg/L MWCNT exposure, respectively (Fig. 4A) indicating disturbance in ROS balance. Similarly, MWCNT exposure at 100 and 500 mg/L concentrations induced significant H_2O_2 accumulation in roots and shoots of Arabidopsis seedlings (Yang et al., 2023). The accumulated H_2O_2 suggests modified detoxifying mechanisms. Using *in situ* detection method, mature root zones showed a sporadic and dot-like pattern of peroxidase activation in *B. napus* in the presence of 80 mg/L MWCNT (Fig. 4B, indicated by an arrow). This is supported by literature where plant peroxidases were induced by MWCNTs (Smirnova et al., 2012; Ghasempour et al., 2019; Chen et al., 2021). However, the *in situ* activation of peroxidases was not observed in the roots of *S. lycopersicum* (Fig. 4B). One of the major H_2O_2 quenchers is APX which activity was significantly increased by both MWCNT dosages in the roots of both species (Fig. 4C). Similarly, MWCNT exposure significantly increased APX activity *e.g.* in *Ocimum basilicum*, grape, tomato (Gohari et al., 2020; Li et al., 2022; González-García et al., 2019; López-Vargas et al., 2020). In *B. napus* shoot, abundance of neither of the two APX isoforms (cAPX1, cAPX2) showed changes as the effect of MWCNT treatments (Fig. 4D, Fig. S1). The protein amount of both APX isoforms increased in the roots of 10 mg/L MWCNT-exposed *B. napus*, while the 80 mg/L dose caused elevated protein levels only in case of cAPX2 (Fig. 4D, Fig. S1). In *S. lycopersicum*, only one APX isoform was detected with slight 80 mg/L MWCNT-induced increase in protein level in the shoot (Fig. 4D, Fig. S1). Additionally, the lower MWCNT dosage caused a decrease in APX protein level in the roots of *S. lycopersicum* (Fig. 4D, Fig. S1) which together with the increased total activity (Fig. 4C) indicates that the APX enzyme pool is highly activated in the presence of MWCNT.

In the shoot of *B. napus*, a significant increase in the amount of carbonylated proteins was observed in at least three protein bands (Fig. 5, indicated by arrows, Fig. S2). In the root, only one protein band showed notable MWCNT-associated signal intensification (Fig. 5, indicated by an arrow, Fig. S2) suggesting a moderate change in the active proteome of *B. napus* induced by MWCNT exposure. In contrast, both the shoot and the root proteome of *S. lycopersicum* suffered severe changes in response to MWCNT treatment, since the signal associated with carbonylated proteins increased in several protein bands in both plant organs compared to control (Fig. 5, indicated by arrows, Fig. S2). These are supported by the results of HaiTao et al. (2018) where MWCNTs induced an increase in the amount of carbonylated proteins in *Vicia faba*. It is noteworthy that in the shoot the higher MWCNT concentration, while in the root the lower dosage triggered the protein carbonylation response (Fig. 5, Fig. S2). These suggest the relative sensitivity of the root system possibly due to the direct contact with MWCNTs.

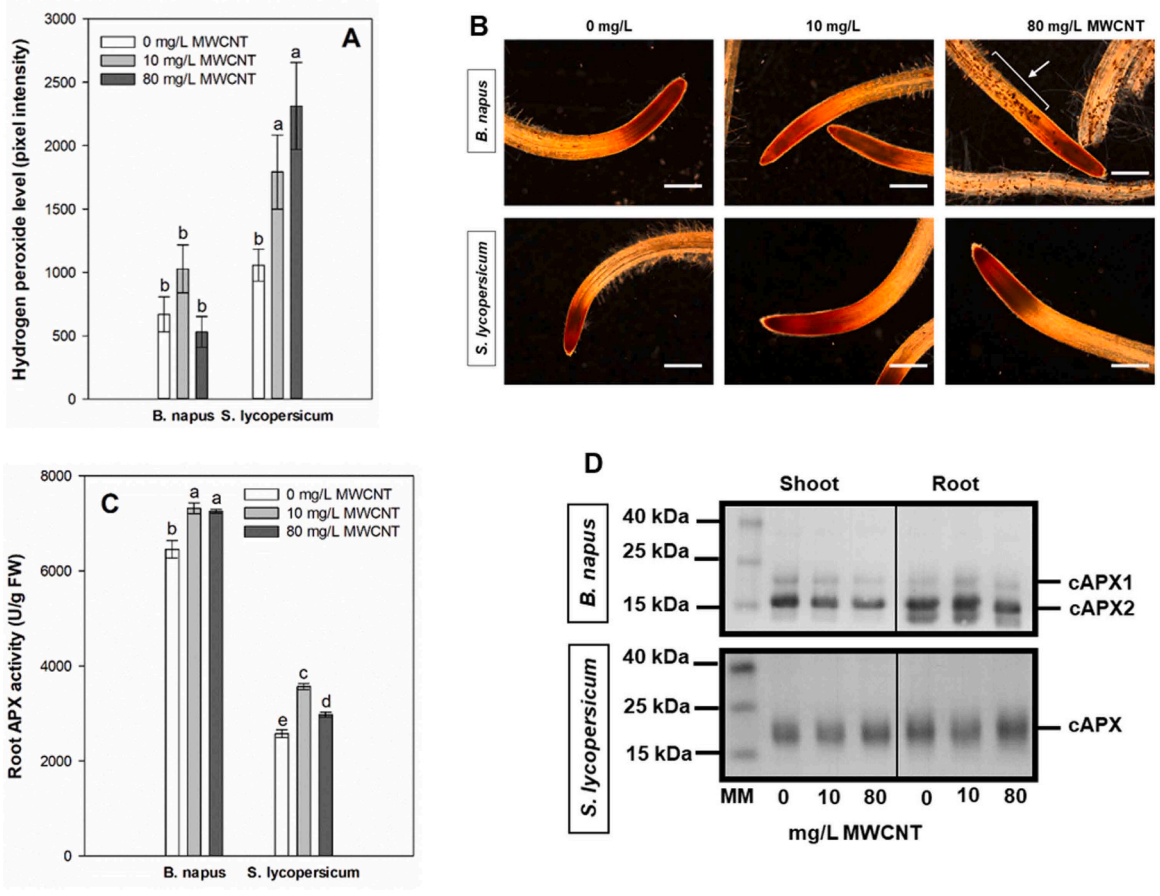

Fig. 4. Hydrogen peroxide levels in the root tips of *B. napus* and *S. lycopersicum* seedlings grown in the presence of 0, 10 or 80 mg/L MWCNT. Data are expressed in pixel intensity, and different letters indicate significant differences according to Duncan's multiple range test ($n = 10$, $P \leq 0.05$). (B) Representative images of root tips stained with pyrogallol. Scale= 250 μm. (C) APX enzyme activity (expressed as unit/ g fresh weight) in root samples. Different letters indicate significant differences according to Duncan's multiple range test ($n = 5$, $P \leq 0.05$). (D) Western blot analysis of APX protein abundance in shoot and root of *S. lycopersicum* and *B. napus* seedlings. MM= molecule marker, cAPX= cytoplasmic APX isoform.

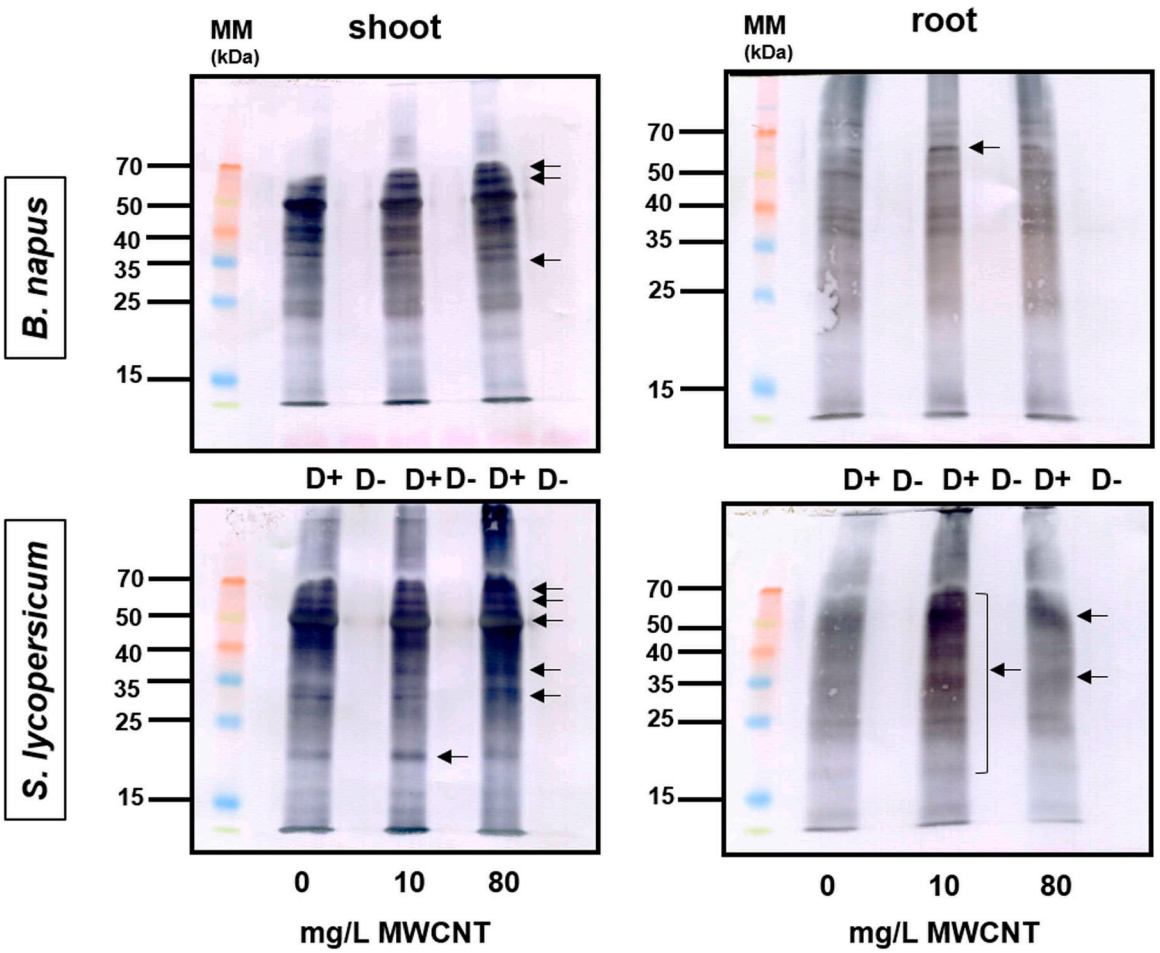

Fig. 5. Western blot analysis of carbonylated proteins in the shoot and root of *B. napus* and *S. lycopersicum* seedlings exposed to 0, 10 or 80 mg/L MWCNT. Protein bands with intensified signal compared to control (0 mg/L MWCNT) are marked with black arrows. MM= molecule marker, D+ =derivatized sample, D-=non-derivatized sample. Non-derivatized samples can be seen as empty lines and were used as negative controls (see Materials and Methods).

3.5. MWCNTs induce significant changes in RNS levels, metabolism and protein nitration

As for NO levels, the 80 mg/L MWCNT concentration caused 23% decrease in *B. napus* roots, while the lower concentration caused no changes compared to control (Fig. 6). Interestingly, *S. lycopersicum* roots showed no changes in endogenous NO levels as the effect of 10 and 80 mg/L MWCNT exposure (Fig. 6). MWCNT in a lower concentration (5 mg/L) caused significant NO accumulation in tomato roots which was accompanied by increased lateral root formation (Cao et al., 2020). The different effect of MWCNT on NO levels may be due to the different treatment concentrations. Cao et al. (2020) used beneficial MWCNT

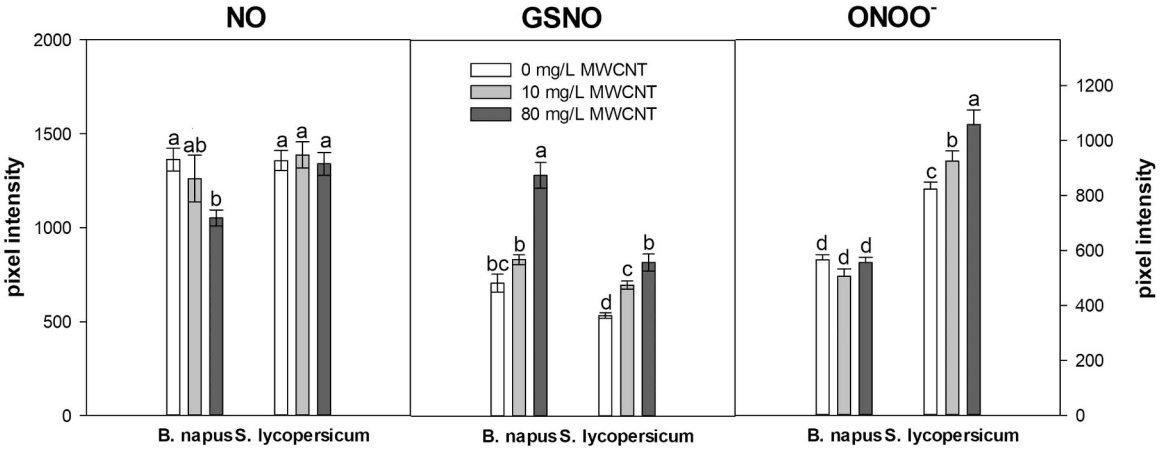

Fig. 6. Nitric oxide (NO), *S*-nitrosoglutathione (GSNO) and peroxynitrite ($ONOO^-$) levels in the roots of 0, 10 or 80 mg/L MWCNT-exposed *B. napus* and *S. lycopersicum*. Data are expressed in pixel intensity, and different letters indicate significant differences according to Duncan's multiple range test ($n = 10$, $P \leq 0.05$).

dosages while in our system the applied concentrations were inhibiting (see Fig. 3). In case of *B. napus* roots, 10 and 80 mg/L MWCNT resulted in ~17% and ~80% elevation in GSNO levels, respectively. In the roots of *S. lycopersicum* seedlings, the MWCNT-induced increases in GSNO levels were ~30 and ~50% (in case of 10 and 80 mg/L MWCNT, respectively) compared to control (Fig. 6). Since the GSNO level increase was accompanied by a MWCNT-induced decrease in NO levels in *B. napus*, we suppose that the formation of GSNO from NO may be induced. In other words, the increase in the amount of GSNO suggests that the roots' RNS pool moves in the direction of the stable, stored and transported form as the effect of MWCNTs. These changes in active RNS pool were species independent in this system. In the roots of *B. napus*, MWCNT treatments resulted in unchanged $ONOO^-$ levels compared to control, while both 10 and 80 mg/L MWCNT doses significantly (by ~12 and ~28%, respectively) increased $ONOO^-$ levels in the roots of *S. lycopersicum* (Fig. 6). This anticipates the possibility of increased protein tyrosine nitration. Indeed, as the effect of MWCNTs, *S. lycopersicum* showed intensification in the physiological nitration of proteins; however, the effects were moderate. Increased immunopositive signals associated with tyrosine nitration were detected in more protein bands, especially in the root (Fig. 7, indicated by arrows, Fig. S3). In the shoot and root of *B. napus* seedlings, no obvious changes in physiological protein nitration compared to control were observable (Fig. 7).

The activity of GSNOR enzyme decreased (by 25%) relative to control in the shoot of 10 mg/L MWCNT-exposed *B. napus*, while in the root system the 80 mg/L dose induced GSNOR activity (by 50%, Fig. 8 A). In *S. lycopersicum* shoot, 10 mg/L MWCNT significantly increased GSNOR activity, while the higher dosage decreased it in both organs (by 13% in the shoot and by 45% in the root, Fig. 8 A). In *S. lycopersicum* root, the reduced GSNOR activity is accompanied by increased GSNO level (Fig. 6.). This indicates that the down-regulation of GSNOR may be responsible for GSNO increase. At the protein level, MWCNT significantly increased GSNOR protein abundance in *B. napus* (Fig. 8B, Fig. S4) which may lead to the increased activity (Fig. 8 A). The GSNOR enzyme could be poorly detected in the samples derived from both organs of *S. lycopersicum* (Fig. 8B, Fig. S4). It has to be noted that 80 mg/L MWCNT resulted in notably enhanced GSNOR protein amount in the roots of *S. lycopersicum* (Fig. 8B, Fig. S4). The relative expression of *GSNOR1* was modified by MWCNT concentrations in neither organ of either species (Fig. 8 C). Nitrate reductase (NR) is a key enzyme in nitrogen metabolism and may also be associated with root NO production (Chamizo-Ampudia et al., 2017). In the roots of *B. napus*, the relative expression of NR encoding *NIA1* increased as the effect of 80 mg/L MWCNT exposure but this did not lead to NO formation. In fact, a reduced NO level was detectable in this sample (see Fig. 6, NO). This suggests that NR is unrelated to NO production in the presence of inhibitory MWCNT doses in contrast to the beneficial dose (Cao et al., 2020). Phytoglobins may regulate endogenous NO levels in a reaction yielding nitrate (Cochrane et al., 2017). The expression of phytoglobin encoding *GLB2* was decreased significantly in *B. napus* roots by both MWCNT doses (Fig. 8 C). Again, the downregulation of *GLB2* was not associated with NO level changes suggesting that *GLB2* may perform a function independent of NO level regulation. In *S. lycopersicum* roots, the expressions of *NIA1* and *GLB2* showed no significant changes compared to control. *Solanum lycopersicum* expresses three *GLB* genes (*GLB1*, *GLB2* and *GLB3*) and *GLB3* proved to be MWCNT-responsive since its relative expression significantly increased in the roots of 80 mg/L MWCNT-exposed plants. Similar to *B. napus*, *GLB3* acts independently from NO level regulations in *S. lycopersicum*.

4. Conclusions

MWCNTs are internalized in root cells and possibly are translocated in the aerial plant parts of *B. napus* and *S. lycopersicum* seedlings. MWCNTs are heavily transformed within the cells forming large

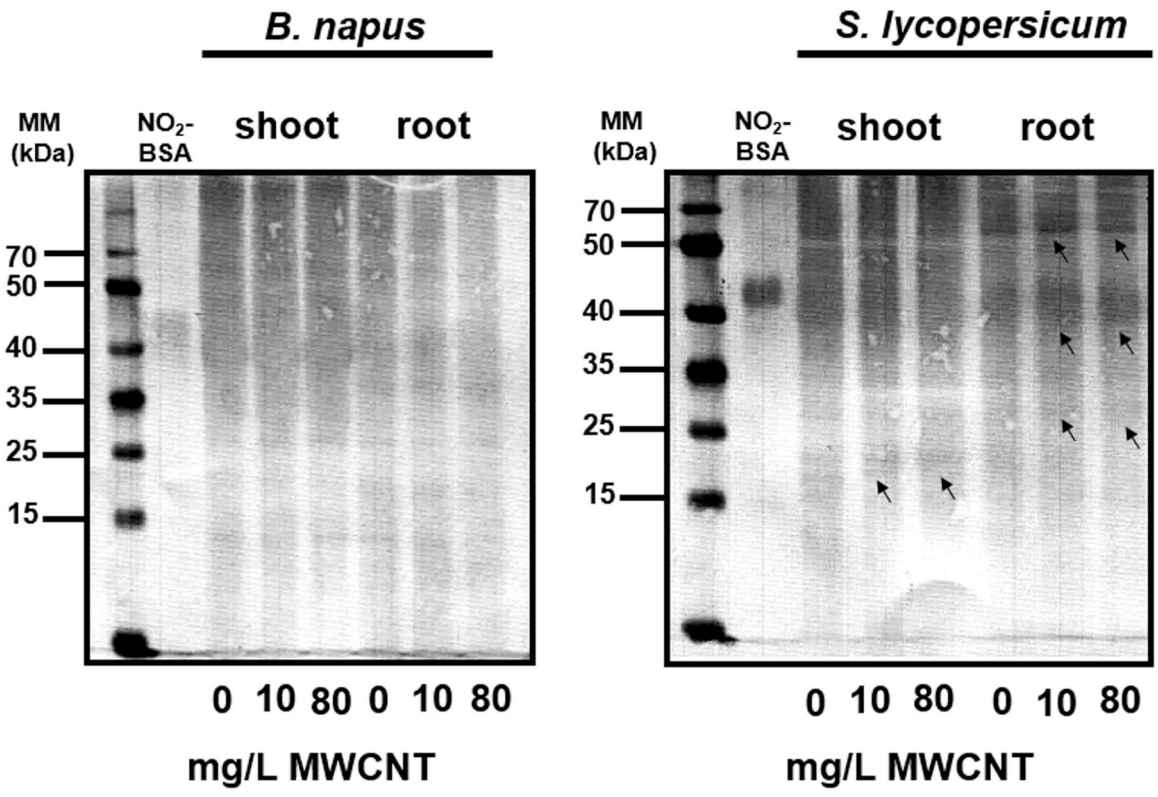

Fig. 7. Western blot analysis of protein tyrosine nitration in *B. napus* and *S. lycopersicum* grown in the presence of 0, 10 or 80 mg/L MWCNT. Protein bands with increased immunopositive signal are marked with small black arrows. NO_2-BSA (nitrated bovine serum albumin) served as positive control. The changes in immunopositive signals were slight in *B. napus*, therefore those were not marked by arrows.

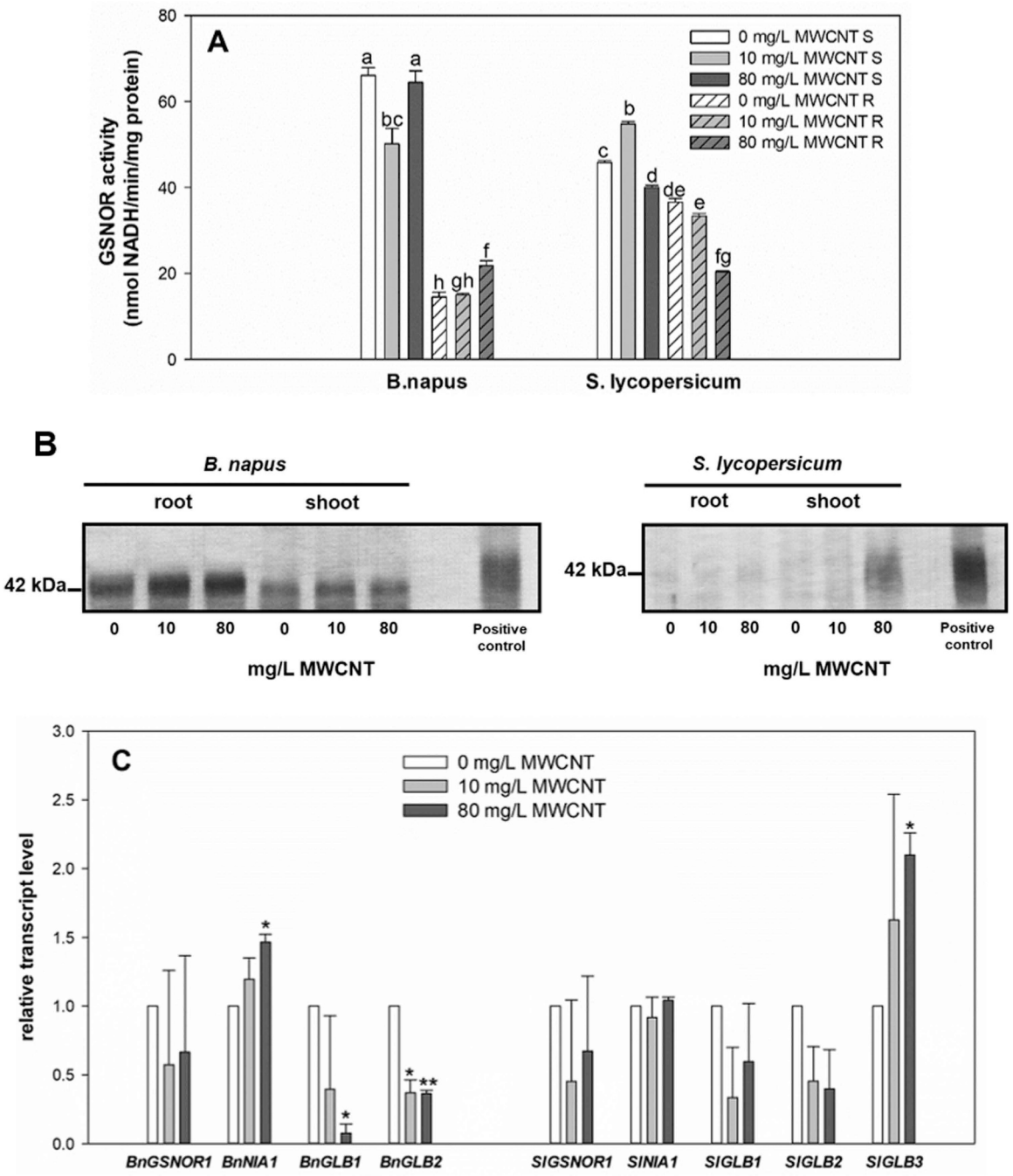

Fig. 8. (A) GSNOR enzyme activity (nmol NADH/min/mg protein) in the root and shoot of 0, 10 or 80 mg/L MWCNT-exposed *B. napus* and *S. lycopersicum* seedlings. Different letters indicate significant differences according to Duncan's multiple range test ($n = 5$, $P \leq 0.05$). (B) Representative western blot showing GSNOR protein abundance in the shoot and root of *B. napus* and *S. lycopersicum* seedlings. Protein extract from GSNOR overproducer *35S::FLAG-GSNOR1* Arabidopsis seedlings served as positive control. (C) Relative expression levels of selected NO-associated genes in the roots of *B. napus* and *S. lycopersicum* in response to MWCNT treatments. Significant differences are indicated by asterisks according to Student t-test ($n = 3$, $^*P \leq 0.05$; $^{**}P \leq 0.01$).

aggregates likely with attached macromolecules. The uptake of MWCNTs negatively affects key cellular processes in both species but the toxicity proved to be more intense in *S. lycopersicum* compared to *B. napus.* MWCNT-induced protein carbonylation is more intense in the relative sensitive *S. lycopersicum*, where this is accompanied by a large increase in H_2O_2 levels. Additionally, we first demonstrated that MWCNT exposure induces protein tyrosine nitration which proved to be more intense in *S. lycopersicum,* where notable $ONOO^-$ accumulation occurred.

These suggest that MWCNT triggers secondary nitro-oxidative stress which contributes to its toxicity. Moreover, the results indicate that the extent of the nitro-oxidative processes is associated with the extent of MWCNT toxicity.

The understanding of the underlying mechanism of toxicity may contribute to the more reliable risk assessment of nanotubes and to their safe utilization in crop production. However, we have to note that the fate of nanotubes in the soil-plant-human system must be uncovered before introducing them into agricultural practice.

CRediT authorship contribution statement

Zsuzsanna Kolbert: Conceptualization, Funding acquisition,

Supervision, Data curation, Visualization, Writing - original draft, Writing - review & editing. **Árpád Molnár:** Investigation, Data curation, Methodology, Writing - original draft, Writing - review & editing. **Kamilla Kovács:** Investigation, Data curation. **Sára Lipták-Lukácsik:** Investigation, Data curation. **Péter Benkő:** Investigation, Data curation. **Réka Szőllősi:** Investigation, Methodology. **Katalin Gémes:** Supervision, Writing - review & editing. **László Erdei:** Supervision, Writing - review & editing. **Andrea Rónavári:** Investigation, Data curation, Funding acquisition, Writing - original draft, Writing - review & editing. **Zoltán Kónya:** Supervision, Writing - review & editing.

Declaration of Competing Interest

The authors declare the following financial interests/personal relationships which may be considered as potential competing interests: Zsuzsanna Kolbert reports financial support was provided by National Research, Development and Innovation Office of Hungary. Zsuzsanna Kolbert reports a relationship with National Research, Development and Innovation Office of Hungary that includes: board membership.

Data Availability

Data will be made available on request.

Acknowledgements

The authors would like to thank Dr. Zsolt Rázga† for his valuable help in TEM analyses and Éva Kapásné Török for her help during the laboratory works. This work was supported by the National Research, Development and Innovation Office of Hungary under grant No. K 135303 (Zs.K.) and PD 143320 (A.R.).

Appendix A. Supporting information

Supplementary data associated with this article can be found in the online version at doi:10.1016/j.ecoenv.2023.115633.

References

Abdel-Ghani, N.T., El-Chaghaby, G.A., Helal, F.S., 2015. Individual and competitive adsorption of phenol and nickel onto multiwalled carbon nanotubes. J. Adv. Res 6, 405–415.

Cao, Z., Zhou, H., Kong, L., Li, L., Wang, R., Shen, W., 2020. A novel mechanism underlying multi-walled carbon nanotube-triggered tomato lateral root formation: the involvement of nitric oxide. Nanoscale Res. Lett. 15, 49 https://doi.org/10.1186/s11671-020-3276-4.

Chaki, M., Valderrama, R., Fernández-Ocaña, A.M., et al., 2009. Protein targets of tyrosine nitration in sunflower (*Helianthus annuus* L.) hypocotyls. J. Exp. Bot. 60, 4221–4234.

Chamizo-Ampudia, A., Sanz-Luque, E., Llamas, A., Galvan, A., Fernandez, E., 2017. Nitrate reductase regulates plant nitric oxide homeostasis. Trend Plant Sci. 22, 163–174.

Chen, G., Qiu, J., Liu, Y., et al., 2015. Carbon nanotubes act as contaminant carriers and translocate within plants. Sci. Rep. 5, 15682 https://doi.org/10.1038/srep15682.

Chen, J., Zeng, X., Yang, W., et al., 2021. Seed priming with multiwall carbon nanotubes (MWCNTs) modulates seed germination and early growth of maize under cadmium (Cd) toxicity. J. Soil Sci. Plant Nutr. 21, 1793–1805.

Cherati, S.R., Shanmugam, S., Pandey, K., Khodakovskaya, M.V., 2021. Whole-transcriptome responses to environmental stresses in agricultural crops treated with carbon-based nanomaterials. ACS Appl. Biol. Mater. 4, 4292–4301.

Cochrane, D.W., Shah, J.K., Hebelstrup, K.H., Igamberdiev, A.U., 2017. Expression of phytoglobin affects nitric oxide metabolism and energy state of barley plants exposed to anoxia. Plant Sci. 265, 124–130.

Corpas, F.J., Carreras, A., Esteban, F.J., Chaki, M., Valderrama, R., del Río, L.A., Barroso, J.B., 2008. Localization of *S*-nitrosothiols and assay of nitric oxide synthase and *S*-nitrosoglutathione reductase activity in plants. Method. Enzym. 437, 561–574.

Corpas, F.J., González-Gordo, S., Palma, J.M., 2021. Protein nitration: a connecting bridge between nitric oxide (NO) and plant stress, 2, 100026. https://doi.org/10.1016/j.stress.2021.100026.

Eleftheriou, E.P., Adamakis, I.D.S., Panteris, E., Fatsiou, M., 2015. Chromium-induced ultrastructural changes and oxidative stress in roots of *Arabidopsis thaliana*. Int. J. Mol. Sci. 16, 15852–15871.

Fangue-Yapseu, G.Y., Tola, A.J., Missihoun, T.D., 2022. Proteome-wide analysis of hydrogen peroxide-induced protein carbonylation in *Arabidopsis thaliana*. Front. Plant Sci. 13, 1049681 https://doi.org/10.3389/fpls.2022.1049681.

Ghasempour, M., Iranbakhsh, A., Ebadi, M., Ardebili, Z.O., et al., 2019. Multi-walled carbon nanotubes improved growth, anatomy, physiology, secondary metabolism, and callus performance in *Catharanthus roseus*: an *in vitro* study. 3 Biotech 9, 404. https://doi.org/10.1007/s13205-019-1934-y.

Gohari, G., Safai, F., Panahirad, S., Akbari, A., Rasouli, F., Dadpour, M.R., Fotopoulos, V., 2020. Modified multiwall carbon nanotubes display either phytotoxic or growth promoting and stress protecting activity in *Ocimum basilicum* L. in a concentration-dependent manner. Chemosphere 249, 126171. https://doi.org/10.1016/j.chemosphere.2020.126171.

González-García, Y., López-Vargas, E.R., Cadenas-Pliego, G., et al., 2019. Impact of carbon nanomaterials on the antioxidant system of tomato seedlings. Int. J. Mol. Sci. 20, 5858. https://doi.org/10.3390/ijms20235858.

HaïTao, L., Run, W.C., Ling, L., YunYun, L., Yun, Y., KangKang, L., 2018. Oxidative damages of carboxylated multi-walled carbon nanotubes, lead and cadmium in the leaves of *Vicia faba* seedlings. J. Ecol. Rural. Environ. 34, 745–754.

Hao, Y., Yu, F., Lv, R., et al., 2016. Carbon nanotubes filled with different ferromagnetic alloys affect the growth and development of rice seedlings by changing the C:N ratio and plant hormones concentrations. PLoS ONE 11, e0157264. https://doi.org/10.1371/journal.pone.0157264.

He, H., Pham-Huy, L.A., Dramou, P., Xiao, D., Zuo, P., Pham-Huy, C., 2013. Carbon nanotubes: applications in pharmacy and medicine. Biomed. Res. Int. 2013, 578290 https://doi.org/10.1155/2013/578290.

Hu, Y., Zhang, P., Zhang, X., et al., 2021. Multi-Wall carbon nanotubes promote the growth of maize (*Zea mays*) by regulating carbon and nitrogen metabolism in leaves. J. Agric. Food Chem. 69, 4981–4991.

Jahnová, J., Luhová, L., Petřivalský, M., 2019. *S*-nitrosoglutathione reductase- The master regulator of protein *S*-nitrosation in plant NO signaling. Plants 8, 48. https://doi.org/10.3390/plants8020048.

Khalifa, N.S., 2018. The effect of multi-walled carbon nanotubes on pennycress (*Thlaspi arvense* L.) plant. Egypt. J. Bot. 58, 529–537.

Khodakovskaya, M.V., Kim, B.-S., Kim, J.N., Alimohammadi, M., Dervishi, E., Mustafa, T., Cernigla, C.E., 2013. Carbon nanotubes as plant growth regulators: effects on tomato growth, reproductive system, and soil microbial community. Small 9, 115–123.

Kolbert, Zs, Pető, A., Lehotai, N., Feigl, G., Ördög, A., Erdei, L., 2012. *In vivo* and *in vitro* studies on fluorophore-specificity. Acta Biol. Szeged 56, 37–41.

Kolbert, Zs, Feigl, G., Bordé, Á., Molnár, Á., Erdei, L., 2017. Protein tyrosine nitration in plants: present knowledge, computational prediction and future perspectives. Plant Physiol. Biocem 113, 56–63.

Kolbert, Zs, Molnár, Á., Szőllősi, R., Feigl, G., Erdei, L., Ördög, A., 2018. Nitro-oxidative stress correlates with se tolerance of Astragalus species. Plant Cell Physiol. 59, 1827–1843.

Lahiani, M.H., Dervishi, E., Chen, J.H., Nima, Z., Gaume, A., Biris, A.S., et al., 2013. Impact of carbon nanotube exposure to seeds of valuable crops. ACS Appl. Mater. Interfaces 5, 7965–7973.

Larue, C., Pinault, M., Czarny, B., et al., 2012. Quantitative evaluation of multi-walled carbon nanotube uptake in wheat and rapeseed. J. Hazard. Mater. 227–228, 155–163.

Li, B., Sun, C., Lin, X., Busch, W., 2021. The emerging role of GSNOR in oxidative stress regulation. Trend Plant Sci. 26, 156–168.

Li, Y., Liu, M., Yang, X., Zhang, Y., Hui, H., Zhang, D., Shu, J., 2022. Multi-walled carbon nanotubes enhanced the antioxidative system and alleviated salt stress in grape seedlings. Sci. Hortic. 293, 110698 https://doi.org/10.1016/j.scienta.2021.110698.

Lin, C., Fugetsu, B., Su, Y., Watari, F., 2009. Studies on toxicity of multi-walled carbon nanotubes on Arabidopsis T87 suspension cells. J. Hazard. Mater. 170, 578–583.

Lin, C., Su, Y., Takahiro, M., Fugetsu, B., 2010. Multi-walled carbon nanotubes induce oxidative stress and vacuolar structure changes to Arabidopsis T87 suspension cells. Nano Biomed. 2, 170–181.

Liu, Q., Chen, B., Wang, Q., Shi, X., Xiao, Z., Lin, J., Fang, X., 2009. Carbon nanotubes as molecular transporters for walled plant cells. Nano Lett. 9, 1007–1010.

López-Vargas, E.R., González-García, Y., Pérez-Álvarez, M., Cadenas-Pliego, G., González-Morales, S., Benavides-Mendoza, A., Cabrera, R.I., Juárez-Maldonado, A., 2020. Seed priming with carbon nanomaterials to modify the germination, growth, and antioxidant status of tomato seedlings. Agronomy 10, 639. https://doi.org/10.3390/agronomy10050639.

Martínez-Ballesta, M.C., Zapata, L., Chalbi, N., Carvajal, M., 2016. Multiwalled carbon nanotubes enter broccoli cells enhancing growth and water uptake of plants exposed to salinity. J. Nanobiotechnol. 14, 42 https://doi.org/10.1186/s12951-016-0199-4.

Mathew, S., Tiwari, D.K., Tripathi, D., 2021. Interaction of carbon nanotubes with plant system: a review. Carbon Lett. 31, 167–176.

Molnár, Á., Papp, M., Kovács, D.Z., et al., 2020. Nitro-oxidative signalling induced by chemically synthetized zinc oxide nanoparticles (ZnO NPs) in Brassica species. Chemosphere 251, 126419. https://doi.org/10.1016/j.chemosphere.

Nakano, Y., Asada, K., 1981. Hydrogen peroxide is scavenged by ascorbate specific peroxidase in spinach chloroplasts. Plant Cell Physiol. 22, 867–880.

Nakayama, H., Kawade, K., Tsukaya, H., Kimura, S., 2015. Detection of the cell proliferation zone in leaves by using EdU. Bio-Protoc. 5, e1600 https://doi.org/10.21769/BioProtoc.1600.

Rahmani, N., Radjabian, T., Soltani, B.M., 2020. Impacts of foliar exposure to multi-walled carbon nanotubes on physiological and molecular traits of *Salvia verticillata* L., as a medicinal plant. Plant Physiol. Biochem. 150, 27–38.

Safdar, M., Kim, W., Park, S., Gwon, Y., Kim, Y.-O., Kim, J., 2022. Engineering plants with carbon nanotubes: a sustainable agriculture approach. J. Nanobiotechnol. 20, 275 https://doi.org/10.1186/s12951-022-01483-w.

Sakamoto, A., Ueda, M., Morikawa, H., 2002. Arabidopsis glutathione-dependent formaldehyde dehydrogenase is an *S*-nitrosoglutathione reductase. FEBS Lett. 515, 20–24.

Smajda, R., Kukovecz, Á., Kónya, Z., Kiricsi, I., 2007. Structure and gas permeability of multi-wall carbon nanotube buckypapers. Carbon 45, 1176–1184.

Smirnova, E., Gusev, A., Zaytseva, O., et al., 2012. Uptake and accumulation of multiwalled carbon nanotubes change the morphometric and biochemical characteristics of *Onobrychis arenaria* seedlings. Front. Chem. Sci. Eng. 6, 132–138.

Szőllősi, R., Molnár, Á., Kondak, S., Kolbert, Zs, 2020. Dual effect of nanomaterials on germination and seedling growth: stimulation *vs.* phytotoxicity. Plants 9, 1745. https://doi.org/10.3390/plants9121745.

Tola, A.J., Jaballi, A., Missihoun, T.D., 2021. Protein carbonylation: emerging roles in plant redox biology and future prospects. Plants 10, 1451. https://doi.org/10.3390/plants10071451.

Valderrama, R., Corpas, F.J., Carreras, A., et al., 2007. Nitrosative stress in plants. FEBS Lett. 581, 453–461.

Yang, S., Yin, R., Wang, C., Yang, Y., Wang, J., 2023. Phytotoxicity of zinc oxide nanoparticles and multi-walled carbon nanotubes, alone or in combination, on *Arabidopsis thaliana* and their mutual effects on oxidative homeostasis. PLoS ONE 18, e0281756. https://doi.org/10.1371/journal.pone.0281756.

Yang, Z., Deng, C., Wu, Y., et al., 2021. Insights into the mechanism of multi-walled carbon nanotubes phytotoxicity in Arabidopsis through transcriptome and m6A methylome analysis. Sci. Total Environ. 787, 147510 https://doi.org/10.1016/j.scitotenv.2021.147510.

Ye, J., Coulouris, G., Zaretskaya, I., Cutcutache, I., Rozen, S., Madden, T., 2012. Primer-BLAST: a tool to design target-specific primers for polymerase chain reaction. BMC Bioinfo 13, 134. https://doi.org/10.1186/1471-2105-13-134.